

Flow of the normal component of He-II about bluff objects observed with He₂^{*} excimers

X. Wen^{1,2,3}, J. Pierce,² N. Lavrik,⁴ S. J. Randolph,⁴ W. Guo^{5,6}, and M. R. Fitzsimmons^{1,2,3,*}

¹*Department of Physics and Astronomy, University of Tennessee, Knoxville, Tennessee 37996, USA*

²*Oak Ridge National Laboratory, Oak Ridge, Tennessee 37830, USA*

³*Shull Wollan Center—a Joint Institute for Neutron Sciences, Oak Ridge, Tennessee 37830, USA*

⁴*Center for Nanophase Materials Sciences, Oak Ridge National Lab, Oak Ridge, Tennessee 37830, USA*

⁵*Mechanical Engineering Department, FAMU-FSU College of Engineering, Florida State University, Tallahassee, Florida 32310, USA*

⁶*National High Magnetic Field Laboratory, Tallahassee, Florida 32310, USA*



(Received 20 October 2022; revised 26 December 2022; accepted 19 April 2023; published 2 May 2023)

Flow of the normal fluid component of He II about a cylinder and flat plate in a channel with a square cross-section was observed by tracking clouds of He₂^{*} excimers. Flow was produced using a lithographically patterned heater. The direction and speed of flow projected onto a plane parallel to the axis of the channel and perpendicular to the heater exhibited significant change with time even after the heater was turned off. Flow was recorded in movies. Excimers moved at least as fast as could be recorded by the camera. Velocity vector field maps of flow suggest formation of structures downstream of the cylinder object that are consistent with parts of eddies. In this paper, we establish a foundation to observe normal component flow of a quantum fluid over centimeters.

DOI: [10.1103/PhysRevB.107.174501](https://doi.org/10.1103/PhysRevB.107.174501)

I. INTRODUCTION

Previously, Zhang and Van Sciver [1] observed flow of He II about a cylindrical bluff object using particle image velocimetry (PIV) [2–5] to record motion of many 1.7- μm -diameter polymer spheres. The spheres, bluff object, and He II were contained inside a channel-shaped cuvette. To induce flow, a heater at the bottom of the cuvette was energized and the surface of the He II actively pumped (cooled) to 2 K. For low heater power, smooth eddyless flow was observed about the object. For high power, pairs of eddies in the wake and, remarkably, in front of the object (the latter displaced to the sides of cuvette) were observed. Eddies in the wake of the object are expected for strong flow of a classical fluid; however, eddies in front of the object are not consistent with classical flow. Speculation at the time was that turbulence in front of the object was a manifestation of the unique properties of thermal counterflow between normal and superfluid components of He II.

Sergeev and Barenghi [6] analyzed two-dimensional Euler fluid flow past a disk. Using classical fluid dynamics, they obtained stationary solutions which allowed them to qualitatively conclude that quantized eddies exist upstream and downstream of the disk like those observed in Ref. [1]. Notably, mutual friction between normal and superfluid vortices was not required to produce eddies for the duration of the experiments. However, mutual friction would be required for quantized vortices to induce eddies in the normal component.

Later, Chagovets and Van Sciver [7] reproduced the essential results of the previous experimental study—namely, observation of smooth eddyless flow for lightly driven counterflow and eddies in front of and behind the cylinder for strongly

driven counterflow. For their work, He II was seeded with 1–5- μm -diameter solid H₂ spheres, and the motion of individual spheres were tracked using particle tracking velocimetry (PTV) [8–11]. PTV enabled Chagovets and Van Sciver [7] to observe H₂ tracers dragged by the normal fluid component of He II and tracers trapped by quantum vortices in the superfluid component. Tracers in the two components were observed to move in opposite directions, demonstrating thermal counterflow.

Later, Duda *et al.* [12] reported experimental results of thermal counterflow of He II past opaque and transparent cylinders using solid H₂ tracers under conditions like those in Refs. [1,7]. Duda *et al.* [12] observed eddies in front and in the wake of the cylinder when the data were analyzed using PIV. However, they found no evidence for eddies in front of the object when the motion of the H₂ tracers was tracked using PTV. They suggested PIV tended to report vortices when none were observed with PTV. We note the observations of vortices were consistent for applications of PIV and PTV reported in Refs. [1,7].

Numerical simulations of thermal counterflow in He II about a cylinder provided insight into the physics leading to the formation of turbulence in a quantum fluid. Soullaine *et al.* [13] found that, for a ratio of superfluid (ρ_s) to normal fluid (ρ_n) densities $a = \frac{\rho_s}{\rho_n} < 1$, friction between the normal fluid component and the boundaries of the cuvette and object could induce eddies in the wake of the object for flow corresponding to modest heater power in Refs. [1,7,12]. For higher power, if the product of a and the mutual friction between normal fluid and superfluid components γ was sufficiently large, then eddies formed in front of the object. These simulations qualitatively explained the observations in Refs. [1,7]. Namely, mutual friction between superfluid and normal fluid components of He II is critical for the manifestation of turbulence in front of a cylindrical bluff object. Understanding flow in such

*mfitzs1@utk.edu

a fluid is important for applications such as cryogenic cooling of complex objects, e.g., accelerators [14], or components having porous materials [15] (to maximize surface area in contact with the cooling medium).

A complexity of the experimental work to date is that massive tracers interact with both normal fluid and superfluid components of He II. Therefore, it is difficult to uniquely identify the origin of the eddies upstream of the cylinder. Do the eddies exist in the normal fluid component, or are the tracers trapped in polarized quantized vortices of the superfluid component? For temperatures > 1 K, He_2^* excimers are only entrained by the normal fluid component [16–22], so He_2^* excimer tracers can clarify the origin of eddies upstream of a cylinder in He II [23–26]. Other advantages of He_2^* excimer tracers in comparison with massive particles are (1) the fluid can be seeded with excimers with less concomitant heating, and (2) interactions between excimers are relatively weak. For example, massive tracers may acquire electrostatic charge through friction between the gas flow and the injection-nozzle wall. We note electrostatic interactions are widely studied and exploited in the materials science of self-assembled small inorganic and organic (including polymeric) structures [27–30].

In our two previous publications, we reported a technique to produce He_2^* excimer molecules with neutron beams to seed a $1 \times 1 \times 1$ cm³ volume of He II at the bottom of a long cuvette with a square cross-section [31] and to observe thermally induced flow of excimer tracers in a channel filled with He II [32]. Through visual inspection of the fluorescence from He_2^* excimers, the excimers, and thus flow of the normal fluid component of He II, were observed to move vertically up the channel of the cuvette away from the energized heater at the bottom of the cuvette. In addition, a machine learning (ML) algorithm identified clusters of excimers. The centroids of the clusters were tracked in a manner akin to PTV. The results yielded a velocity vector flow field (in two dimensions) across an Eulerian grid. Here, we extend our studies to flow of the normal component of He II about two kinds of bluff objects—a cylinder and a flat plate. Because cooling the liquid/vapor surface opposite to the heater is not practical for our experiment (it is too expensive to pump and discard ³He), the conditions in Refs. [1,7,12] cannot be faithfully reproduced. Thus, the long-term goal to determine whether eddies upstream of a cylinder occur only in the normal fluid component remains an outstanding challenge. Nevertheless, in this paper, we document (1) the responsiveness of excimers to track the normal component of flow around objects on short (ms) time scales, (2) the consistency between raw recordings of the motion of excimer fluorescence around objects and velocity vector field maps obtained using ML and correlation analysis from the recordings, and (3) changes to the instrumentation that would yield an environment more closely replicating those described in Refs. [1,7,12] while preserving ³He. In this paper, we lay the foundation for future examination of the origin of eddies upstream of a cylinder bluff object using ML and recordings of He_2^* excimer fluorescence.

II. METHODS

A detailed description of the experimental setup is given in Refs. [31,32]. Briefly, an Oxford OptistatCF2 cryostat (a

static exchange gas continuous flow cryostat) with quartz windows transparent to infrared light contained a 3.5-cm-long quartz cuvette with a 1×1 cm² cross-section. The cuvette was connected to a 3.5-L reservoir filled with a mixture of ³He and ⁴He in the ratio of 1:99 (pressure was 97 kPa at 300 K). The cuvette was immersed in the liquid He bath (nominal temperature of 1.6 K), and the contents of the cuvette were cooled through the five walls of the cuvette.

The instrumentation for the experiment (Fig. 1) is most like that described in Ref. [32]; notably, a BN beam blocker (outside the cryostat) blocked the neutron beam from entering the top half of the field of view of the camera. A 343 Ω (at room temperature) labyrinth microheater was fabricated by photolithographically patterning gold onto a fused silica wafer. The wafer was subsequently diced into 2.5×7.5 mm² chips [Fig. 1(c)] that were secured to G10 pucks—only one was required for an experiment. The labyrinth was energized using a constant current source and provided a source of heat uniformly distributed across its 1.8×7 mm² (plated) surface. The long dimension of the heater was parallel to the focal plane, laser plane, and neutron beam incident vector [Fig. 1(b)]. The heater was attached to a G10 rod and located 6 mm from the bottom of the cuvette. The G10 rod was displaced behind the focal plane by ~ 2 mm. A bluff object (either a 2-mm-diameter glass cylinder 4 mm long, or a 1-mm-thick $\times 4 \times 6$ mm² glass plate) was attached to the G10 rod ~ 6 mm above the heater [Fig. 1(d)].

Because the liquid/vapor interface of the ³He : ⁴He mixture was not actively pumped, the interface was not a cooling interface; thus, the flow of heat inside the cuvette may not be as simple as if the interface had been actively cooled. Nevertheless, as shown in Ref. [32], in the absence of a bluff object, the motion of the excimers is upward, implying the normal fluid component of He II flowed away from the heat source.

III. RESULTS

We collected ~ 27 s of data taken at a rate of 55.6 Hz for heater powers of $P = 0, 2.5, 5, 7.5, 10, 15, 20, 30, 40, 60, 80,$ and 100 mW (heat flux $q = P/A$, where $A = 0.13$ cm² is the cross-section of the heater). Up to three 27-s-long measurements were taken for each power. All measurements used the same timing sequence: $t = 5$ s neutron shutter open, $t = 8$ s camera recording start, $t = 10$ s lasers on, $t = 14$ s heater on, $t = 18$ s heater off, and $t = 35$ s recording stop. During image acquisition, the temperature and ³He : ⁴He vapor pressure sensors were recorded every 0.5 s. Prior to turning the heater on, the temperature of the cuvette equilibrated between 1.5 and 1.8 K. Just after the heater was turned off ($t = 18$ s), the temperature of the cuvette increased by not more than 0.3 K compared with the temperature at $t = 14$ s. In addition, a measurement with the neutron shutter closed (so no excimers were produced) and with the heater off was made using the same timing protocol. This measurement quantified the background, which was removed from the excimer fluorescence images in the manner described in the supplemental material of Ref. [32].

He_2^* excimers were excited by 905-nm pulses with 4-ns duration at a rate of 1 kHz (9 mJ per pulse). Immediately

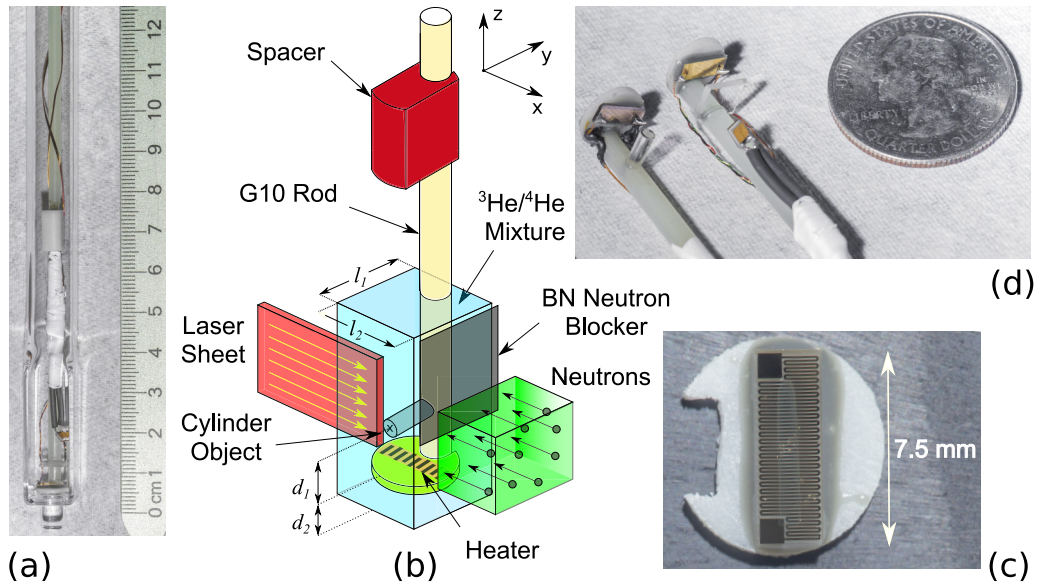


FIG. 1. (a) Cuvette with sample rod, heater, and flat plate inserted. (b) Schematic arrangement of the cuvette with respect to laser and neutron beams ($l_1 = l_2 = 10$ mm). The labyrinth heater (c) is $d_2 \sim 6$ mm from the bottom of the cuvette (a). (d) Sample rods with glass cylinder and flat plate bluff objects installed $d_1 \sim 6$ mm from the heater.

after a pulse, each excimer will emit a 640-nm photon. We recorded the 640-nm fluorescence from He_2^* excimers during a 30- μs interval at a rate of 55.6 Hz with a camera that was synchronized with the laser. Because a photon has only a 1 in 42 chance of entering the solid angle subtended by the camera lens, we cannot continuously track individual excimers from frame to frame [32]. Because tens of thousands of excimers are created in a region reasonably confined by the path lengths of the proton and tritons (produced by ^3He absorption of a neutron), the excimers form clouds. Instead of tracking individual excimers, we track the fluorescence from clouds or clusters of excimers. Clusters of excimers were identified using an unsupervised ML algorithm, and the centroids of the clusters were tracked from frame to frame using a correlation metric [32]. A velocity vector flow field was constructed from the cluster/correlation analysis.

A. Nonuniformity of illumination—Origin and consequences

Excimer fluorescence in the 1×1 cm² field of view mapped onto a 1024×1024 array of pixels (high-resolution mode) was recorded for > 19 s about the cylinder [Fig. 2(a)] and flat plate [Fig. 2(b)]. These recordings were made without applying power to the heater. The boundaries of the objects are highlighted by continuous white lines in the figures. Inside the regions occupied by the objects, there are no excimers, and hence, they appear dark. To the right of the objects and between the dashed lines in the figures are regions that are generally darker than elsewhere. The regions of diminished fluorescence result from the loss of 905-nm laser light (the laser light needed to excite the excimers) due to refraction of the beam by the bluff object. The nonuniformity occurs rapidly across the dashed lines. The sudden loss of excimer fluorescence may affect the clustering algorithm, e.g., the calculation of the cluster centroid may be shifted outside the affected region where there is more light. We regard the

velocity vector fields (shown later) just to the right of the objects to be less reliable than elsewhere.

The second nonuniformity of the light is the gradual increase of light from left to right. This nonuniformity is a consequence of the absorption of the neutron beam by ^3He (the absorption length is ~ 4 mm for the concentration of ^3He and the average of the neutron beam wavelength from 2.8 to 5.8 Å [33]). As the neutron beam travels through the cell, the beam is absorbed, so there are fewer He_2^* excimers produced on the left than the right; consequently, there are fewer excimers to fluoresce. Because the loss of fluorescence is gradual, the loss will not lead to erroneous results in clustering or the process to identify cluster motion. However, because there is less light on the left than the right, there are fewer clusters to follow the flow on the left, so the uncertainty of the flow will be larger on the left than the right.

B. Flow of He II about a cylinder observed with He_2^* excimers

To record flow of He II about the cylinder, a power P was selected for the heater, and a recording was made using the time sequence described earlier. For recordings of flow, the BN neutron beam blocker was placed outside the cryostat to the right of the field of view of the camera. The blocker was positioned so that only the region of the cuvette for vertical position < 1 mm was illuminated by the neutron beam. We call the region below +1 mm the excimer creation zone. Because excimers are not created above this zone, fluorescence above the zone must come from excimers that have moved upward from the excimer creation zone into the shadow of the neutron beam.

Figure 3 shows images recorded with only background light subtracted—the latter measured with neutron beam shutter closed and heater off. Otherwise, the images were minimally processed. Figure 3(a) is a collection of measurements from three experiments taken from $t = 10$ to 14 s when the

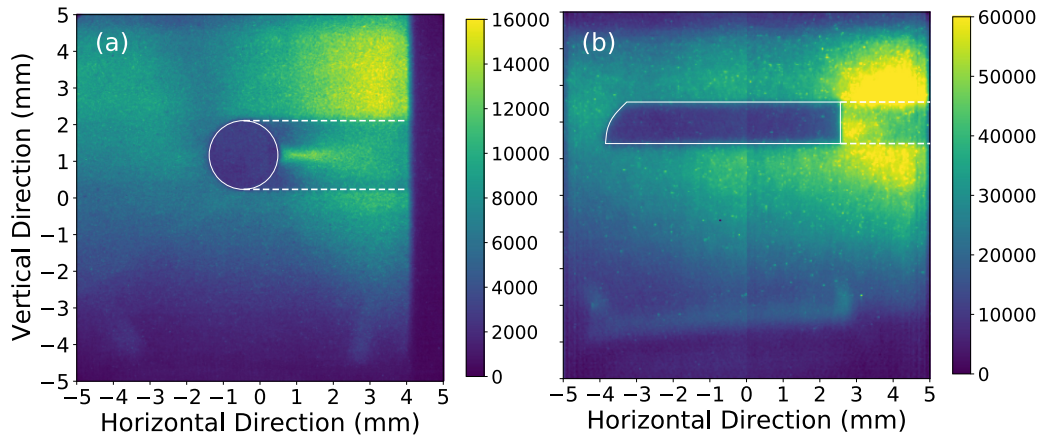


FIG. 2. Exposure taken of He_2^* excimer fluorescence around the (a) cylinder (duration = 19 s) and (b) flat plate (duration = 25 s) bluff objects (outlined by continuous white lines). The 905-nm light used to excite the He_2^* excimers was refracted by the objects accounting for the nonuniformity of the fluorescence to the right of the objects and between the dashed lines. The BN neutron beam blocker was removed to acquire these images. The color bar shows the number of counts recorded in a pixel during the exposure. Counts are proportional to the charge accumulated by the pixel. Charge is proportional to the intensity of the fluorescence.

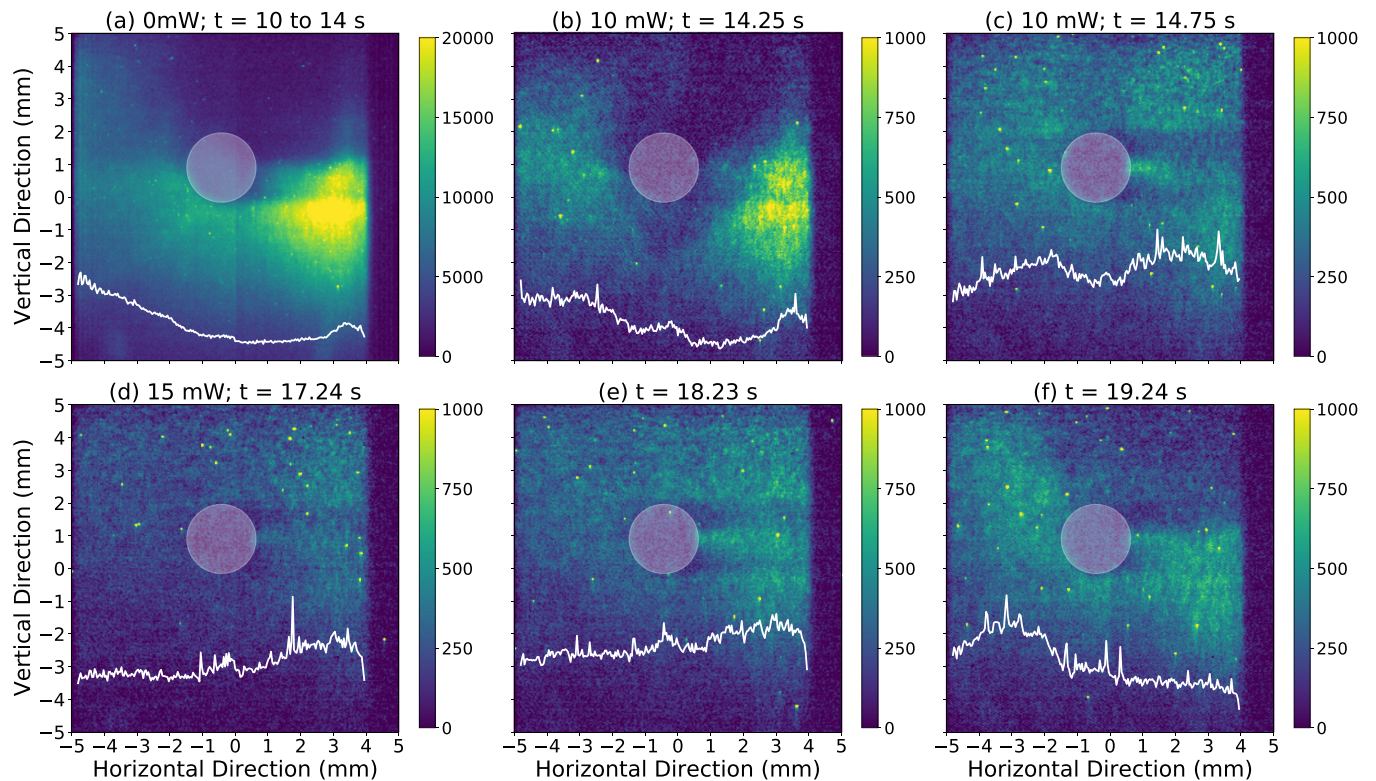


FIG. 3. (a) Image for $P = 0$ mW integrated over the first 4 s. The upper half of the field of view is in the shadow of the neutron beam blocker (the beam blocker is to the right of the cryostat outside the field of view). Absence of light in this region implies the absence of flow. Images for $P = 10$ mW integrated over a period of 0.5 s. These images show the wake of the cylinder devoid of light for (b) $t = 14.25$ s and then filling with light from excimers that flowed into the wake for (c) $t = 14.75$ s. (b) and (c) were obtained from frames of the raw recording used to make Movie S1 in the Supplemental Material [35]. A sequence of images for a measurement starting with $P = 15$ mW (heater is on from $t = 14$ to 18 s) integrated over a period of 0.5 s showing (d) low intensity of light in the upper half of the field of view, (e) more light with increasing intensity from left to right in the upper half, and (f) reversal of the distribution of light from left to right in the upper half compared with (d), thus evidence for circulation of excimer light and flow of the normal fluid component of He II around the cylinder. (d)–(f) were obtained from frames of the raw recording used to make Movie S2 in the Supplemental Material [35]. The white lines show the intensity integrated over vertical direction > 2 mm vs horizontal direction. The scale of the white line ranges from zero to the same maximum for (b)–(f). The scale for (a) is $\frac{1}{20}$ th the scale for (b)–(f).

heater was off. This figure shows fluorescence was strongest below the neutron beam shadow, i.e., in the excimer creation zone. In this zone, the intensity on the right is higher (yellow color) than the left (light green color), which is consistent with increasing absorption of the neutron beam from right to left. The relative absence of fluorescence in the neutron shadow (above the object) indicates the lack of flow to carry He_2^* excimers from the bottom to the top of the cuvette when the heater is off; however, diffusion of He_2^* excimers from bottom to top still occurs, contributing to some light in the neutron beam shadow. The diffusion length for He_2^* excimers at 1.6 K during the 5-s period from neutron shutter open to lasers on is ~ 1 mm [34]. The white line in Fig. 3(a) shows the integration of the intensity over vertical position > 2 mm (i.e., above the object) vs horizontal position. The zero of intensity for the line corresponds to the bottom of the figure.

Figures 3(b) and 3(c) are 0.5-s integrations of data corresponding to $P = 10$ mW for times of $t = 14.25$ and 14.5 s, respectively. Figure 3(b) shows the absence of fluorescence in the wake of the cylinder and then filling of the wake with fluorescence in Fig. 3(c). This is evident by the broadly diminished intensity of the white line in Fig. 3(b) corresponding to the integrated intensity in the plane above the object (vertical position > 2 mm). By *wake of the cylinder*, we mean the region above the cylinder and within $\sim \pm 3$ mm of horizontal position = 0 mm. Then for Fig. 3(c), the intensity in the region of vertical position > 2 mm is more uniform vs horizontal position—the broadly diminished intensity seen in Fig. 3(b) being more tightly confined in Fig. 3(c) and the variation vs horizontal position being reduced.

Figures 3(d)–3(f) show a sequence of 0.5-s time integrations of data starting with $P = 15$ mW. Focusing on the upper half of the fields of view for the figures and using the color bar as a guide to intensity of fluorescence, the intensity shown in the first image of the sequence [Fig. 3(d)] is weak overall (in the range of ~ 250 to ~ 500 a.u.). The left side is weaker than the right side, as evident in the variation of the white line (intensity integrated over vertical position > 2 mm) of Fig. 3(d). This observation is consistent with upward flow of the normal fluid component of He II from the excimer creation zone in which there are fewer excimers on the left to trace the flow than the right. The intensity in the second image [Fig. 3(e)] is somewhat stronger (in the range of ~ 375 to ~ 625 a.u.). The profile of the intensity above the object [the white line of Fig. 3(e)] is higher than that of Fig. 3(d), and the variation of the integrated intensity from left to right of the former is somewhat reduced compared with the latter. The intensity in the final image [Fig. 3(f)] is highly nonuniform. The intensity ranges from a low of ~ 100 a.u. on the right side (upper corner) to a high of ~ 750 a.u. on the left side (upper corner). The variation from left to right is opposite that of the first figure for the upper half of the field of view [compare the intensity profiles, i.e., white lines, of Figs. 3(f) and 3(d)]. These images suggest that excimers moved (and thus, the normal fluid component, too) from right to left across the upper half of the field of view. These observations, as best a comparison of static images permit, are consistent with circulation of the normal fluid component flow in a counter-clockwise direction about the cylinder.

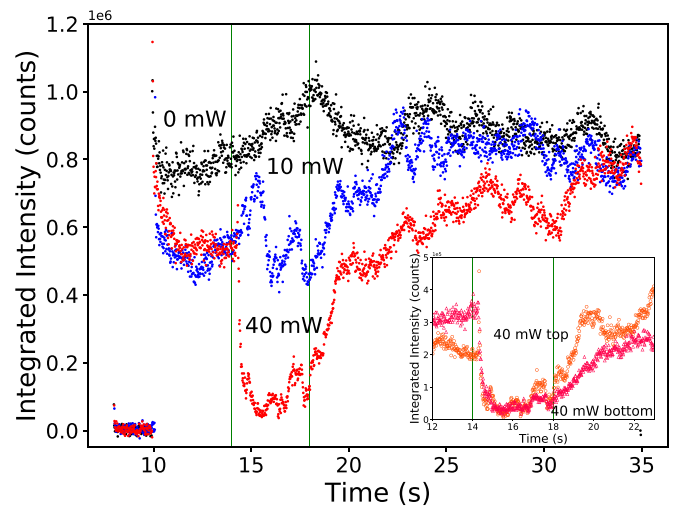


FIG. 4. Intensity integrated over the entire field of view vs time for $P = 0, 10,$ and 40 mW obtained from the cylinder object experiment. The faint green lines at $t = 14$ and 18 s correspond to the times when the heaters were turned on and off, respectively (except for the $P = 0$ mW measurement). (inset) Intensity integrated over the top (orange \circ) and bottom (red \triangle) halves of the field of view vs time for heater power of $P = 40$ mW.

Movies for experiments corresponding to the static images are provided in the Supplemental Material [35]. Data and movies for all powers are available on the Zenodo Website [36]. Inspection of the movies (which is strongly encouraged) provides more clarity of the motion of the excimer light and hence the flow of the normal fluid component of He II. The feature that is most striking from the movies is how rapidly the light moves across the field of view. Notably, however, eddies are not evident from simple inspection of the movies. Defective camera pixels (amounting to 2.5% of the total number) were excluded from the movies. The movies show only excimer peaks with intensities > 3 times the standard deviation of the background measurements (3σ). The excimer peaks in the movies will be used to identify clusters of excimers (discussed later).

The movies (see Supplemental Material [35] and the Zenodo Website [36]) show complex time-dependent flow of the fluorescence that persists after the heater is turned off. Figure 4 shows the intensity of the excimer light integrated over the entire field of view (after background subtraction) and over 0.5-s intervals vs time. For the case of $P = 0$ mW, the intensity varies by $\sim 10\%$. For the cases of $P = 10$ and 40 mW, the intensity varies more significantly. Note the strongly diminished intensity while the heater is on for the case of the $P = 40$ mW data and recovery of the intensity when the heater is turned off. This observation was consistently observed for all measurements taken with $P > 30$ mW for the cylinder object.

C. Cluster analysis to deduce velocity vector flow fields around bluff objects

Velocity vector flow fields (projected onto the focal plane) can be deduced from superposition of many images of tracers that involve calculating cross-correlations between images

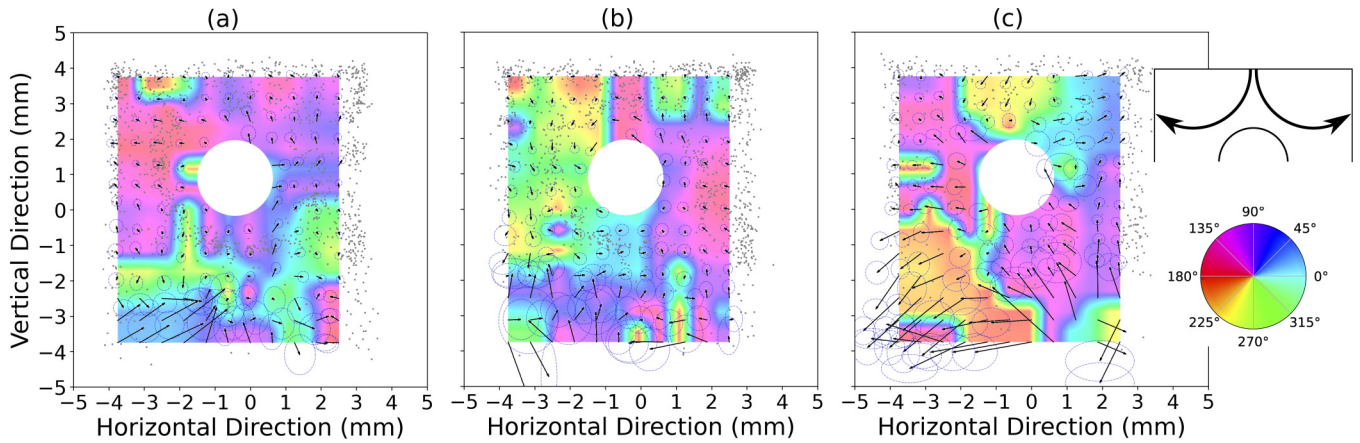


FIG. 5. Correlated cluster pairs about the cylinder object are shown as gray dots for (a) $P = 7.5$ mW, (b) $P = 15$ mW, and (c) $P = 40$ mW. A velocity flow field is shown by the arrows averaged over velocity vectors of the cluster pairs within a 2×2 mm integration window centered at each point of the Eulerian grid. The ellipses represent the uncertainty equal to the standard error of the mean for the vertical and horizontal components of the cluster pair velocities. Color represents the direction of the flow relative to the positive horizontal direction per the color wheel, inset lower right, with up being 90° . The flow as shown by the arrows and associated color in (c) ($P = 40$ mW) is indicated in the schematic, inset upper right.

(PIV) or tracking movement of individual tracers (PTV). Because the photon emitted by an excimer is unlikely to enter the camera, neither PIV nor PTV can be applied to directly track individual excimers for our experiment [32]. Instead, flow was inferred from motion of ensembles (clusters) of excimers since these clusters contain many excimers and can produce enough photons to be recorded by the camera. A velocity vector flow field was deduced from the motion of the centroids accumulated during the time the heater was on (4 s), i.e., the flow field represents the net motion of flow during a 4-s interval.

As described in Ref. [32], we applied an unsupervised ML algorithm to identify clusters of excimer light from every frame. The ML algorithm also returns the centroid of each cluster. A second algorithm (also described in Ref. [32]) identified pairs of centroids that were correlated frame to frame from which a displacement vector for each cluster pair was determined. Using the displacement vector and the frame rate of the camera, 1000+ velocity vectors were obtained for measurements while the heater was on. To facilitate visualization of the vector velocity flow field, an Eulerian grid with a mesh of 1×1 mm² was defined [32], and the average of the velocity vectors in a 2×2 mm² integration window was obtained for each grid point. Results for a selection of heater powers are shown in Fig. 5. The gray dots in the figure show the origin of the velocity vectors for the 1000+ cluster pairs. The black arrows show the direction and magnitude of the velocity for a grid point representing an average of a cluster pair of velocity vectors in the 2×2 mm² integration window. The color wheel shows the direction of the flow in the manner used to show the spatial dependence of the orientation of the vector magnetization of skyrmions [37]. Color is correlated with angle of the flow as measured relative to the horizontal direction pointing from left to right in the usual sense—angle is positive as measured in the counterclockwise direction. For example, a region of the figure colored cyan indicates the flow is moving parallel (0°) to the horizontal axis from left to right. The velocity vector flow field provides a sense of magnitude

and direction of flow compiled from 1000+ measurements over a 4-s period that otherwise might not be discernible by inspection by eye of individual frames in movies.

Observations of normal fluid component flow were also obtained from images using a flat plate bluff object. Figure 6 shows a sequence of images integrated over 0.5 s taken

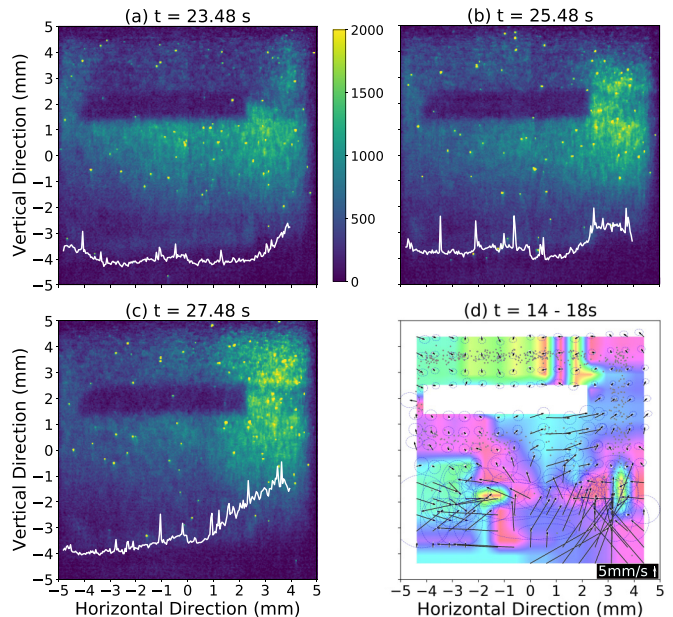


FIG. 6. Excimer fluorescence taken in 2-s intervals showing movement of light from (a) left to (b) right under the flat plate and then upward around the right edge of the plate from (b) to (c) occurring after the heater ($P = 20$ mW) was turned off. (a)–(c) were obtained from frames in Movie S3 in the Supplemental Material [35]. (d) The velocity vector flow field obtained from measurements while the heater was on ($P = 20$ mW) for a 4-s period. For meaning of color (direction of flow), refer to the color wheel shown in the inset of Fig. 5.

at times of (a) $t = 23.48$ s, (b) $t = 25.48$ s, and (c) $t = 27.48$ s. These times occur after the heater for $P = 20$ mW was turned off (recall the heater was turned on at $t = 14$ s for 4 s). These images show (a) fluorescence under the plate, (b) moving upward next to the right edge of the plate, and then (c) along the top of the plate toward the left. The intensity profiles (white lines of intensity integrated over vertical position > 2.5 mm vs horizontal position) show the fluorescence to the right and above the plate increasing from (a) to (b) and then increasing above the plate toward the left of the right edge of the plate in (c). Note these images show motion that persisted after the heater was turned off. The motion of flow can also be observed in the velocity flow field in Fig. 6(d) obtained from data taken while the heater was on. Counterclockwise flow around the right edge of the flat plate is evident by observing how the direction of the velocity vectors [Fig. 6(d)] change as a path is traced starting at the bottom middle of the plate, then moving from left to right under the plate, then moving upward along the right edge, then toward the left around the upper right corner of the plate. Similarly, the color in the region of the right edge of Fig. 6(d), which depicts the direction of the velocity vectors, changes from cyan to blue to magenta to orange in this region transiting the color wheel (inset Fig. 5) in the counterclockwise sense.

IV. DISCUSSION

The still images of Fig. 3 and the field of view integrated intensity vs time plot (Fig. 4) exhibit remarkable changes in the position and intensity of the excimer fluorescence with time. Thus, the flow of the normal fluid component of He II must similarly change with time. Rough estimates for the components of the velocity of excimer motion can be extracted from the data in Fig. 3. For $P = 10$ mW (corresponding to $q = 770$ W/m²) and $t = 14.25$ s, the wake above the cylinder is absent of excimer fluorescence [Fig. 3(b)], and then at $t = 14.5$ s, the region is filled with light [Fig. 3(c)]. Assuming excimers flow into the ~ 6 -mm-wide wake from either side, the horizontal component of the velocity is ~ 6 mm/s ($= \frac{1}{2}6$ mm/0.5 s) for this time interval and power.

For $P = 40$ mW, the intensity of the fluorescence [Fig. 4(c)] changes dramatically. About 80% of the excimer light was lost 0.18 s after the heater was turned on at $t = 14$ s. This implies many excimers left the 1-cm-tall field of view at a rate of ~ 56 mm/s. Then, 1.5 s after the heater was turned off at $t = 18$ s, the intensity recovered its initial value albeit at a slower rate. Because excimer light is a proxy for the flow of the normal fluid component of He II, the flow must rapidly change when the heater is turned on and off.

During the first 4 s of a measurement before the heater was turned on, there is no evidence for flow [Fig. 3(a)]; therefore, we assume for $P = 0$ the velocity of flow is ~ 0 . Fitting values of $v = 6(1)$, $56(6)$ mm/s corresponding to $P = 10(1)$, $40(1)$ mW, respectively, to a line using orthogonal distance regression [38,39] and the constraint $v(0) = 0$ mm/s yields an estimate of velocity in terms of power $v = 1.0(1)P_{\text{mW}}^{\frac{\text{mm}}{\text{s}}}$. This relation provides the reader with an estimate of velocity for a given power. For classical flow, the Reynolds number is given by $\text{Re} = \frac{\rho v D}{\mu}$, where ρ is the density of the medium, μ is the dynamic viscosity of the medium, and D is a length scale

characteristic of an object or channel [40]. Recognizing that He II is a quantum fluid, so application of a classical equation is perhaps dubious (see discussion of this point in Ref. [1]), we nevertheless provide an estimate of Re. Using $\rho = 0.145$ g/cm³ for the total density of the liquid, $\mu = 1.3 \times 10^{-6}$ Pa s (for 1.6 K) [41], and setting $D = 2$ mm (the diameter of the cylinder), we obtain $\text{Re} = 223(20)P/\text{mW}$, which for our experiment means Re ranges from 0 to 22 300. This relation provides the reader with an estimate of the classical Re (of the normal fluid component) for a given power.

Even after the heater was turned off, the intensity of the fluorescence continued to oscillate by $\sim 20\%$ with a period of a couple of seconds (Fig. 4). The diminished intensity for certain times after the heater was turned off means that He₂^{*} excimers moved outside the 1×1 cm² field of view. After a couple of seconds, He₂^{*} excimers reappeared.

There are two sources of He₂^{*} excimers that can repopulate the field of view. One source is the creation of new He₂^{*} excimers in the bottom half of the cuvette (the excimer creation zone). This source can only partially replenish the He₂^{*} excimer population (corresponding to ³He capture of a neutron at a rate of 1 s^{-1}). A second source is recirculation of the normal fluid component of He II from the top of the cuvette toward the bottom of the cuvette, thus bringing He₂^{*} excimers back into the field of view. To test this hypothesis, the $I(t)$ data for $P = 40$ mW are shown in the inset of Fig. 4 integrated across the top (orange \circ) and bottom (red \triangle) halves of the field of view separately. The intensity from the top half of the field of view recovers its $t = 10$ s value 1.5 s after the heater was turned off ($t = 18$ s), whereas the intensity of the bottom half recovers its $t = 10$ s value after 3 s. The factor of 2 longer time for He₂^{*} excimers to repopulate the bottom half of the field of view implies that He₂^{*} excimers primarily come into view from above the field of view (as opposed to having been displaced in front of/behind the laser sheet/focal plane or below the heater). Assuming He₂^{*} excimers move from the middle of the top half (of the field of view) to the middle of the bottom half (a distance of 5 mm) in 1.5 s, then we estimate the speed of the recirculation flow to be ~ 3 mm/s. We associate the rapid loss of excimer fluorescence (corresponding to a velocity of ~ 56 mm/s) for $P > 30$ mW to the heat flux from the heater and the return of the fluorescence when the heater is off to recirculation of flow from above the field of view.

Evolution of flow can add complexity to the interpretation of the velocity vector flow fields in Figs. 5 and 6(d). The flow fields were obtained from observations of cluster-centroid motion during 4-s periods when the heater was on for 1–3 experiments; thus, the flow fields represent the net flow while the heater was on. For the case of Fig. 5(a), the net flow while the heater was on ($P = 7.5$ mW) is upward in the upper right corner corresponding to the blue-purple of the color wheel (90° as measured counterclockwise relative to the positive horizontal direction of the field of view). On the upper left side, the flow is directed to the left side of the cuvette corresponding to red or 180° .

Figures 3(d)–3(f) ($P = 15$ mW) show a sequence of images in which the fluorescence rotates about the cylinder counterclockwise. If these images are representative of the entire 4-s period when the heater was on, then the flow field in Fig. 5(b) ($P = 15$ mW) should also exhibit a similar

trend. Starting from the right side of the cylinder [Fig. 5(b)] and moving counterclockwise around the cylinder, the color changes from purple to red to yellow to green to cyan—circumnavigating the color wheel in a counterclockwise direction. The flow field changes in the same manner as that observed in the still images and the movie of the fluorescence [35,36].

Next, inspection of the rotation of the flow field for $P = 40$ mW starting at the middle of the top of Fig. 5(c), i.e., in the wake of the cylinder, shows a region on the left exhibiting clockwise rotation (yellow to red) and a region on the right exhibiting counterclockwise rotation (yellow to cyan). These counterrotating circulations and structures could be parts of a pair of counterrotating eddies above (i.e., downstream) of the cylinder and centered above the field of view of the camera. The combination of the vector field arrows and change of color above the object in Fig. 5(c) is schematically shown in the upper right inset of the figure. The directions of the circulating flow are such that heat is transported to the cold vertical surfaces of the cuvette to the left and right of the cylinder. The heat flux from the heater for $P = 40$ mW corresponds to 3 kW/m^2 , and the average of the flow velocity magnitude above the cylinder is 2–5 mm/s. (The velocity of flow and the Re for classical flow at high power to produce eddies was noted to be less than that for eddy-free flow at lower power by Ref. [1].) The uncertainty of the flow (i.e., the sizes of the ellipses representing the standard error of the mean of the velocity vectors) is larger than the low-power measurements because there were fewer correlated cluster pairs when the heater was on for $P > 30$ mW (80% of the excimer clusters were swept out of view). Nevertheless, eddies downstream of the cylinder object are anticipated for classical fluids for sufficiently large heat flux [42].

In contrast to Refs. [1,7], we were unable to identify eddies upstream (in front of) the cylinder. There are several reasons why none were seen in our work that motivate future research. First, per the numerical simulations in Ref. [13], a value of $a = \frac{\rho_s}{\rho_n} < 1$ is optimal to generate vortices in the wake of the object; and second, the mutual friction between superfluid and normal components should be large to generate vortices in front of the object. These conditions were fulfilled in Refs. [1,7] which used temperatures of ~ 2 K just below the λ point. Our experiment was performed significantly colder ~ 1.6 K for which $a \sim 5$. Thus, the conditions of our experiment were less conducive to formation of both types of vortices (although some data are consistent with vortices in the wake of the cylinder). In addition, the cuvette used in Refs. [1,7] was optimally suited to produce uniform heat flux by using a heater at the bottom of the cuvette and actively pumping on the liquid/vapor interface at the top. This situation is impossible to achieve using our technique, which requires the He II to be spiked with ^3He ; thus, pumping on the mixture is economically prohibitive. Heat flux in our system may not be as uniform as in Refs. [1,7].

The motion of the fluorescence implies complexity of the transport of He_2^* excimers by the normal fluid component. This is a situation that was not observed by Ref. [1] in recordings of polymer tracers in He II, nor in numerical simulations of Ref. [13] which suggested steady state should be achieved

after ~ 4 s for the conditions in Ref. [1]. *N.B.* we are not saying the previous results lack complexity; rather, we are making a distinction between complexity of trajectories that are stable with time and those that are not.

In comparing our results with those of Ref. [1], we identified a heretofore unremarked feature in data from Ref. [1] arising from the stability of trajectories in time that is absent from our data. Code to produce our analysis of data from Ref. [1] is provided at our GitHub site [43]. Shown in Fig. 7(a) is the integration of 100 images from the movie in the supplemental material in Ref. [1]. A subset of the result is shown in Fig. 7(b). Streaks of intensity, we call filaments, form either linear flow or circulating eddies. The filaments are separated by thin dark (i.e., low intensity) strips. The separation of the filaments in the region corresponding to vertical positions 14–20 mm is $\sim 0.26(2)$ mm, i.e., nearest-neighbor high-intensity filaments are separated by ~ 0.26 -mm-wide regions of low-intensity light. We monitored tracers transiting five pairs of light and dark regions of interest (ROIs) measuring $44 \times 44 \mu\text{m}^2$, as labeled in the image. In Fig. 7(c), we plot the intensity vs time recorded in the light (\bullet) and dark (∇) ROIs (the intensity becomes high as a tracer transits the ROI). We found on average ~ 4 tracers travel through the light ROIs during the 10-s movie in Ref. [1] (~ 1 tracer per 2.5 s) and ~ 1 tracer though the dark ROIs during the same period. From inspection of the movie in Ref. [1], tracer motion in regions corresponding to the light ROIs in Fig. 7(b) exhibit speeds ranging from 4 to 10 mm/s. Using the time of ~ 2.5 s between tracers transiting the light ROIs and the velocity estimate, the spacings of tracers along a filament range from 10 to 25 mm—a large distance compared with the 20-mm width of the channel of Ref. [1]. An explanation could be a single tracer circumnavigates a closed filament (i.e., a loop), or different tracers enter the filament from different directions, e.g., perhaps from outside the focal plane of the camera. In any case, the physical spacing corresponding to tracer(s) transiting ROIs at different times is much larger than the physical separation between filaments, i.e., tens of millimeters compared with a $\frac{1}{4}$ mm, respectively.

In contrast to the images shown in Figs. 7(a) and 7(b), the integration of 200+ frames of a recording from our work ($P = 100$ mW) with comparable heat flux $q = 7.7 \text{ kW/m}^2$ and $\text{Re} \sim 22300$ during a 4-s period from $t = 14$ to 18 s [Fig. 7(d)] shows no evidence for filaments, i.e., we see no tendency for He_2^* excimers to trace special paths. We put forward four hypotheses for the nonuniformity of the trajectories traced by the polymer spheres: (1) The polymer spheres may not have been seeded uniformly into the He II. (2) Repulsive interactions between the spheres, possibly of electrostatic origin, cause the spheres to be distanced from one another. (3) The spheres tend to follow each other for reasons analogous to why cyclists form a peloton (path of least resistance). (4) The trajectories are an example of a recurrent solution to the Navier-Stokes equation for fluid flow [44] realized in Ref. [1] but not by us.

V. CONCLUSIONS

In conclusion, we have observed flow of the normal component of He II around two bluff objects, a cylinder and a

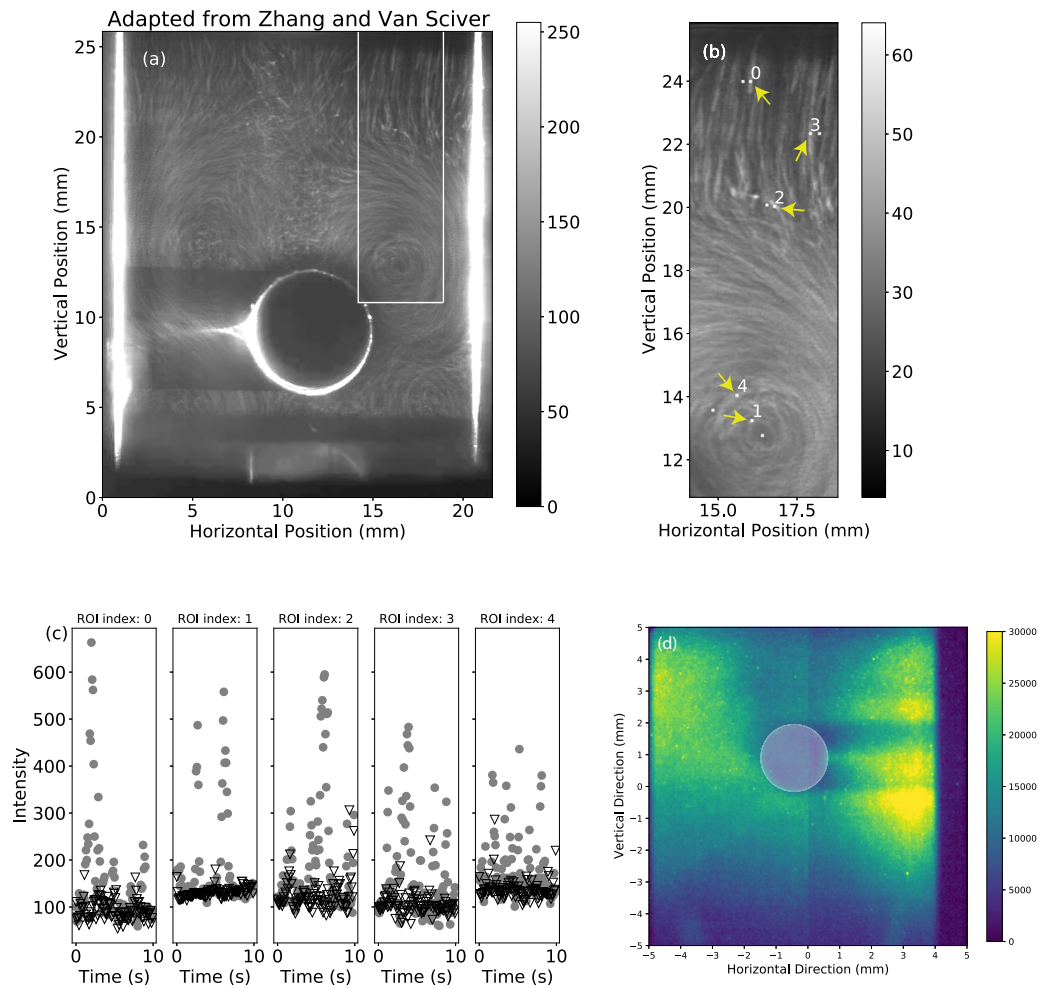


FIG. 7. (a) Integration of 100 images from the movie in Ref. [1] for ($q = 11 \text{ kW/m}^2$, $\text{Re} = 21000$). Region of the white box in (b) shows filaments of high intensity corresponding to light scattered by polymer spheres. The regions are labeled with numbers and pairs of white dots showing the locations of the bright and dark regions of interest (ROIs). The locations of the bright ROIs are shown with arrows. The variations of intensity vs time corresponding to tracers transiting $44 \times 44 \mu\text{m}^2$ ROIs for light (\bullet) and dark (∇) regions labeled in (b) are shown in (c). (d) Integration of 1000 images recorded for our experiment with conditions of $P = 100 \text{ mW}$ ($q = 7.7 \text{ kW/m}^2$, $\text{Re} \sim 27000$) applied for 4 s during the 27-s measurement. Filaments were not observed in the He_2^* excimer fluorescence.

flat plate, by recording the motion of fluorescence of He_2^* excimers. For conditions of 1.6 K and heat flux of $q = 3 \text{ kW/m}^2$ ($P = 40 \text{ mW}$) producing thermal counterflow, we detected counterrotating circulations of flow with a tangential speed of 2–5 mm/s in the wake the cylinder bluff. These circulations could be parts of eddies downstream of the cylinder bluff. The classical Re for this condition is estimated to be ~ 8900 . We observed significant changes to the motion of excimer fluorescence and hence the normal component flow of He II with time, i.e., a steady state was not achieved during recordings lasting $\sim 27 \text{ s}$. Even after the heater was turned off, the intensity of the fluorescence oscillated by $\sim 20\%$ every couple of seconds. For the cylinder study and high power, e.g., $P > 30 \text{ mW}$, $\sim 80\%$ of the He_2^* excimers were swept out of the field of view in $\sim 0.2 \text{ s}$, corresponding to a speed of tens of millimeters per second. The number of He_2^* excimers in the field of view recovered $\sim 1 \text{ s}$ after the heater was turned off. We attribute rapid changes of He_2^* excimer population (in the field of view) to the small inertia of the He_2^* excimers and their exclusive entrainment in the normal fluid component of He II,

so they respond to rapid changes of flow of the normal fluid component about bluff objects in our cuvette. In this paper, we demonstrated the responsiveness of He_2^* excimers to track changing conditions of the flow of the normal fluid component of He II and application of ML and correlation analysis to extract quantitative time-averaged two-dimensional velocity vector flow fields around objects.

Recently, we acquired images of a neutron beam using a next-generation event mode (Photonis brand [45]) camera with a Timepix3 [46] chip. The camera had picosecond time resolution and consisted of 256×256 pixels with $55 \times 55 \mu\text{m}^2$ pixel size and a maximum detection rate of 80 MHz integrated over the field of view [47]. The data collection requirements for the neutron beam demonstration far exceed those needed for the excimer experiment. With new technology, we expect an increase of performance (and signal collection) by the ratio of the laser frequency to the frequency of the camera used presently of $1000 \text{ Hz}/56 \text{ Hz} = 18$. A further $20\times$ gain of signal can be achieved by using more ^3He and optimizing the field

of view and camera lens. Together the $\sim 360\times$ increased signal will improve the reliability of the clustering analysis strategy. An increased data acquisition rate (to 1 kHz) will also improve the reliability of the correlation analysis strategy and extend our ability to observe the responsiveness of excimers to changes of flow that occur in 1 ms instead of 18 ms.

Development and use of the lithographically patterned flat plate heater yielded more uniform heating than the coil heater used previously (see Ref. [32]). However, the lack of a cold surface opposite to the heater frustrates establishment of uniform heat flow for comparison with other work. One means to achieve such flow is to place the heater above the object and replace the glass bottom of the cuvette with a Cu plate. Owing to the low melting point of Cu compared with glass, the simple solution of making a glass-to-Cu seal at the bottom of the cuvette is not feasible. However, a glass-to-stainless-steel flange could be fabricated and an Indium seal used to connect a Cu plate to the stainless flange. This change would require a larger cryostat, yet the size of such a cryostat could still be

smaller than the cross-section of the neutron beam (which can be $\sim 100\text{ cm}^2$ large).

ACKNOWLEDGMENTS

This paper used resources at the Spallation Neutron Source, a U.S. Department of Energy (DOE), Office of Science User Facility operated by the Oak Ridge National Laboratory (ORNL). ORNL is managed by UT-Battelle, LLC, under Contract No. DE-AC05-00OR22725. Fabrication of the labyrinth heater was supported by the Center for Nanophase Materials Sciences, which is a DOE, Office of Science User Facility at ORNL. X.W. acknowledges support from the Shull Wollan Center Graduate Research Fellowship program and the Graduate Advancement, Training and Education program of University of Tennessee. W.G. acknowledges the support from the National Science Foundation under Grant No. DMR-2100790 and the National High Magnetic Field Laboratory, which is supported by National Science Foundation Cooperative Agreement No. DMR-2128556 and the State of Florida.

-
- [1] T. Zhang and S. W. Van Sciver, *Nat. Phys.* **1**, 36 (2005).
- [2] R. J. Adrian and J. Westerweel, *Particle Image Velocimetry* (Cambridge University Press, Cambridge, 2011).
- [3] M. Raffel, C. Willert, S. Wereley, and J. Kompenhans, *Particle Image Velocimetry: A Practical Guide* (Springer-Verlag, Berlin, 2007).
- [4] R. D. Keane and R. J. Adrian, *Appl. Sci. Res.* **49**, 191 (1992).
- [5] R. J. Donnelly, A. N. Karpetsis, J. J. Niemela, K. R. Sreenivasan, W. F. Vinen, and C. M. White, *J. Low Temp. Phys.* **126**, 327 (2002).
- [6] Y. A. Sergeev and C. F. Barenghi, *J. Low Temp. Phys.* **156**, 268 (2009).
- [7] T. V. Chagovets and S. W. Van Sciver, *Phys. Fluids* **25**, 105104 (2013).
- [8] D. Dabiri and C. Pecora, *Particle Tracking Velocimetry* (IOP Publishing, Bristol, UK, 2019).
- [9] K. Ohmi and H.-Yu Li, *Meas. Sci. Technol.* **11**, 603 (2000).
- [10] S. J. Baek and S. J. Lee, *Exp. Fluids* **22**, 23 (1996).
- [11] Y. Tang, S. Bao, T. Kanai, and W. Guo, *Phys. Rev. Fluids* **5**, 084602 (2020).
- [12] D. Duda, M. La Mantia, M. Rotter, and L. Skrbek, *J. Low Temp. Phys.* **175**, 331 (2014).
- [13] C. Soullaine, M. Quintard, B. Baudouy, and R. Van Weelden, *Phys. Rev. Lett.* **118**, 074506 (2017).
- [14] P. Lebrun and L. Tavian, in *Proceedings of the CAS-CERN Accelerator School: Superconductivity for Accelerators* (CERN, Geneva, 2014), pp. 453–476.
- [15] S. W. K. Yuan, T. C. Nast, and T. H. K. Frederking, in *Advances in Cryogenic Engineering*, edited by R. W. Fast (Springer, Boston, 1990), Vol. 35, pp. 197–204.
- [16] A. Marakov, J. Gao, W. Guo, S. W. Van Sciver, G. G. Ihas, D. N. McKinsey, and W. F. Vinen, *Phys. Rev. B* **91**, 094503 (2015).
- [17] J. Gao, W. Guo, V. S. L'vov, A. Pomyalov, L. Skrbek, E. Varga, and W. F. Vinen, *JETP Lett.* **103**, 648 (2016).
- [18] J. Gao, W. Guo, and W. F. Vinen, *Phys. Rev. B* **94**, 094502 (2016).
- [19] J. Gao, E. Varga, W. Guo, and W. F. Vinen, *Phys. Rev. B* **96**, 094511 (2017).
- [20] J. Gao, E. Varga, W. Guo, and W. F. Vinen, *J. Low Temp. Phys.* **187**, 490 (2017).
- [21] J. Gao, W. Guo, S. Yui, M. Tsubota, and W. F. Vinen, *Phys. Rev. B* **97**, 184518 (2018).
- [22] S. Bao, W. Guo, V. S. L'vov, and A. Pomyalov, *Phys. Rev. B* **98**, 174509 (2018).
- [23] D. E. Zmeev, F. Pakpour, P. M. Walmsley, A. I. Golov, W. Guo, D. N. McKinsey, G. G. Ihas, P. V. E. McClintock, S. N. Fisher, and W. F. Vinen, *Phys. Rev. Lett.* **110**, 175303 (2013).
- [24] W. F. Vinen, *AIP Conf. Proc.* **850**, 169 (2006).
- [25] W. Guo, *J. Low Temp. Phys.* **196**, 60 (2019).
- [26] D. Mateo, J. Eloranta, and G. A. Williams, *J. Chem. Phys.* **142**, 064510 (2015).
- [27] N. R. Visaveliya and J. M. Köhler, *Adv. Func. Mater.* **31**, 2007407 (2021).
- [28] F. Nan, F. Han, N. F. Scherer, and Z. Yan, *Adv. Mater.* **30**, 1803238 (2018).
- [29] S. Li, B. A. Moosa, J. G. Croissant, and N. M. Khashab, *Ang. Chemie* **54**, 6804 (2015).
- [30] Z. Zhu, N. Xu, Yu Q. L. Guo, H. Cao, X. Lu, and Y. Cai, *Macromol. Rapid Comm.* **36**, 1521 (2015).
- [31] X. Wen, S. Bao, L. McDonald, J. Pierce, G. L. Greene, L. Crow, X. Tong, A. Mezzacappa, R. Glasby, W. Guo, and M. R. Fitzsimmons, *Phys. Rev. Lett.* **124**, 134502 (2020).
- [32] X. Wen, L. McDonald, J. Pierce, W. Guo, and M. R. Fitzsimmons, *Sci. Rep.* **12**, 20383 (2022).
- [33] <https://www.ncnr.nist.gov/resources/activation/>.
- [34] W. Guo, D. N. McKinsey, A. Marakov, K. J. Thompson, G. G. Ihas, and W. F. Vinen, *J. Low Temp. Phys.* **171**, 497 (2013).
- [35] See Supplemental Material at <http://link.aps.org/supplemental/10.1103/PhysRevB.107.174501> for fabrication of the heater, captions for the three movies and a black/white image of Fig. 5(c).

- [36] X. Wen, J. Pierce, N. Lavrik, S. J. Randolph, W. Guo, and M. R. Fitzsimmons, Zenodo (2022), doi: [10.5281/zenodo.7199829](https://doi.org/10.5281/zenodo.7199829).
- [37] X. Z. Yu, Y. Onose, N. Kanazawa, J. H. Park, J. H. Han, Y. Matsui, N. Nagaosa, and Y. Tokura, *Nature (London)* **465**, 901 (2010).
- [38] http://www.mechanicalkern.com/static/odr_ams.pdf.
- [39] <https://github.com/mfitzsimmons44/Fit-a-polynomial-to-data>.
- [40] A. Sommerfeld, Ein Beitrag zur hydrodynamischen Erklaerung der turbulenten Fluessigkeitsbewegungen, in *Proceedings of the 4th International Congress of Mathematicians* (IMU, Rome, 1908), Vol. 3, pp. 116–124.
- [41] R. J. Donnelly and C. F. Barenghi, *J. Phys. Chem. Ref. Data* **27**, 1217 (1998).
- [42] D. J. Tritton, in *Physical Fluid Dynamics* (Springer, Dordrecht, 1977), pp. 18–29.
- [43] <https://github.com/xwen0518/Flow-of-the-normal-component-of-He-II-about-bluff-objects-observed-with-He-excimers>.
- [44] C. J. Crowley, J. L. Pughe-Sanfor, W. Toler, M. C. Krygier, R. O. Grigoriev, and M. F. Schatz, *Proc. Natl. Acad. Sci.* **119**, e2120665119 (2022).
- [45] <https://www.amscins.com/asi-photonis-joint-venture/>.
- [46] <https://kt.cern/technologies/timepix3>.
- [47] <https://zenodo.org/record/7231893>.